Environ Earth Sci (2016)75:1222
DOI 10.1007/s12665-016-6026-2

ORIGINAL ARTICLE

Specific conductance–stage relationships in Appalachian valley fill streams

Elyse V. Clark[1] · Breeyn M. Greer[2] · Carl E. Zipper[1] · Erich T. Hester[2]

Received: 16 May 2016 / Accepted: 23 August 2016

Abstract Surface coal mining impacts on water resources in the Appalachian region, USA, are widely studied. Total dissolved solids (TDS), which are estimated in situ by the proxy variable specific conductance (SC), are of interest due to potential aquatic macroinvertebrate effects. Prior studies have documented the hydrochemical impacts of surface mining on streams, but research on the relationships between SC and discharge is limited. SC–Stage relationships can help infer potential hydrologic flow paths, as well as source water TDS concentrations in mining-influenced watersheds. The objectives of this study were to compare baseflow and stormflow hydrochemistry and determine SC–Stage relationships in valley fill (VF) streams. Five VF streams of varying ages in Virginia were equipped with continuous SC and stage data loggers for up to 12 months (December 2013–November 2014). Data analyses included baseflow and stormflow hydrochemistry, and SC–Stage regressions and storm hysteresis patterns. Data were analyzed seasonally. Stages were generally highest in winter and lowest in summer, while SCs were generally highest in summer and lowest in winter. All SC–Stage regressions indicated SC dilution during stormflow, but significance differed seasonally. Storm SC–Stage hysteresis patterns varied with storm precipitation amounts, season, and vegetative period, implying climatic controls on VF stream storm responses. Counterclockwise storm hysteresis likely occurred in response to high rainfall amounts exceeding the mine soil infiltration capacity. Clockwise storm hysteresis likely resulted from precipitation dissolving salts brought to the surface by evapotranspiration, but may have also resulted from rapid flow through pseudokarst features within the VF.

Keywords Coal mining · Hysteresis · Reclamation · Specific conductance

Introduction

Land disturbances by mining impact water resources globally by altering hydrologic flow pathways, discharge patterns, and water quality (Atanackovic et al. 2013; Evans et al. 2015; Huang et al. 2010; Younger and Wolkersdorfer 2004). Stream hydrologic and chemical impacts are especially of interest in the Appalachian coalfields of eastern USA, as the surface mining process has disturbed >6000 km^2 of land in the region since the late 1970s (Zipper et al. 2011). Surface waters from mining-influenced watersheds often drain through valley fills (VF), which are landforms constructed of mining-disturbed rocks (mine spoils) that are placed in valleys adjacent to the mining excavations. Individual VFs often cover >10 ha (Evans et al. 2014), and thousands of VFs have been constructed in the Appalachian region (US EPA 2003, 2011).

Coal surface mines with VFs have numerous impacts on water resources and water quality in the Appalachian coalfields (Evans et al. 2014; Messinger and Paybins 2003; Negley and Eshleman 2006; Phillips 2004). During and after VF construction, environmental O_2 and water interact

✉ Elyse V. Clark
eclark2@vt.edu

[1] Department of Crop and Soil Environmental Sciences, Virginia Polytechnic Institute and State University, 185 Ag. Quad Lane, Blacksburg, VA 24061, USA

[2] Department of Civil and Environmental Engineering, Virginia Polytechnic Institute and State University, 200 Patton Hall, Blacksburg, VA 24061, USA

Published online: 03 September 2016

with the freshly mined spoils, initiating rapid spoil weathering. Rainwater leaches soluble ions from the mine spoils, resulting in water discharges with elevated concentrations of dissolved ions which are collectively termed total dissolved solids (TDS). The predominant components of TDS in Appalachian mined streams are SO_4^{2-}, HCO_3^-, Ca^{2+}, and Mg^{2+} (Hartman et al. 2005; Pond et al. 2008; Timpano et al. 2015), and other ions at lower concentrations (Skousen et al. 2000). Total dissolved solids of mine water discharges are typically estimated in situ by the proxy electrical conductivity (EC), and by specific conductance (SC), which is EC corrected to a standard 25 °C and highly correlated to TDS (Timpano et al. 2010).

Typical SCs in discharges from Appalachian VFs range from <500 to >3000 µS cm^{-1} (Evans et al. 2014; Hartman et al. 2005; Pond et al. 2008, 2014), whereas forested streams in unmined watersheds generally have SCs <200 µS cm^{-1} (Boehme et al. 2016; Lindberg et al. 2011; Pond et al. 2008, 2014; Timpano et al. 2015). Elevated SCs in VF streams may alter aquatic macroinvertebrate community assemblages relative to unmined streams due to organism sensitivity to elevated ion concentrations (Boehme et al. 2016; Pond et al. 2008, 2014; Timpano et al. 2015), and these effects have been reported to occur at SCs >300 µS cm^{-1} (Cormier et al. 2013) and ≥500 µS cm^{-1} (Pond et al. 2008).

Although some aspects of VF hydrology and chemistry are documented (Miller and Zegre 2014), few studies have used VF discharges to characterize potential source waters and their associated TDS contributions to streams. Thus, integrative approaches such as concentration–discharge (C–Q) analyses are needed to improve the understanding of the source waters responsible for TDS release to VF streams. C–Q relationships describe changes in streamwater chemistry as discharge varies in response to precipitation and are useful tools for inferring hydrologic flow paths, source waters, basin characteristics, and surface disturbances (Bonta 2004; Evans and Davies 1998; House and Warwick 1998; Rice et al. 2004; Stump 2001). C–Q regressions assist in understanding the chemical- or ion-supply dynamics to streams (i.e., concentration increases or decreases during precipitation events) and have been used to assess watershed land disturbances (Bonta 2004; Lewis and Grant 1979) and temporal trends in hydrochemistry (Murdoch and Shanley 2006). C–Q hysteresis is also used to understand streamwater ion-supply dynamics. During precipitation events, hydrologic systems with C–Q hysteresis generally have a loop pattern, indicating differential discharge timing of a water quality property (e.g., SC, temperature, pH) relative to the rise and fall of water level (Evans and Davies 1998; Walling and Webb 1980).

Hysteresis patterns have been interpreted in a two-component context (Fig. 1a) in which hysteresis results from the differential discharge timing of pre-event and event water (Williams 1989), and in a three-component context (Fig. 1b) in which hysteresis patterns are interpreted to indicate differential discharge timing of the three following hydrograph components: overland flow (*of*), baseflow (*bf*), and soil water (*so*) (Evans and Davies 1998). In the context of VF hydrology, the *so* component

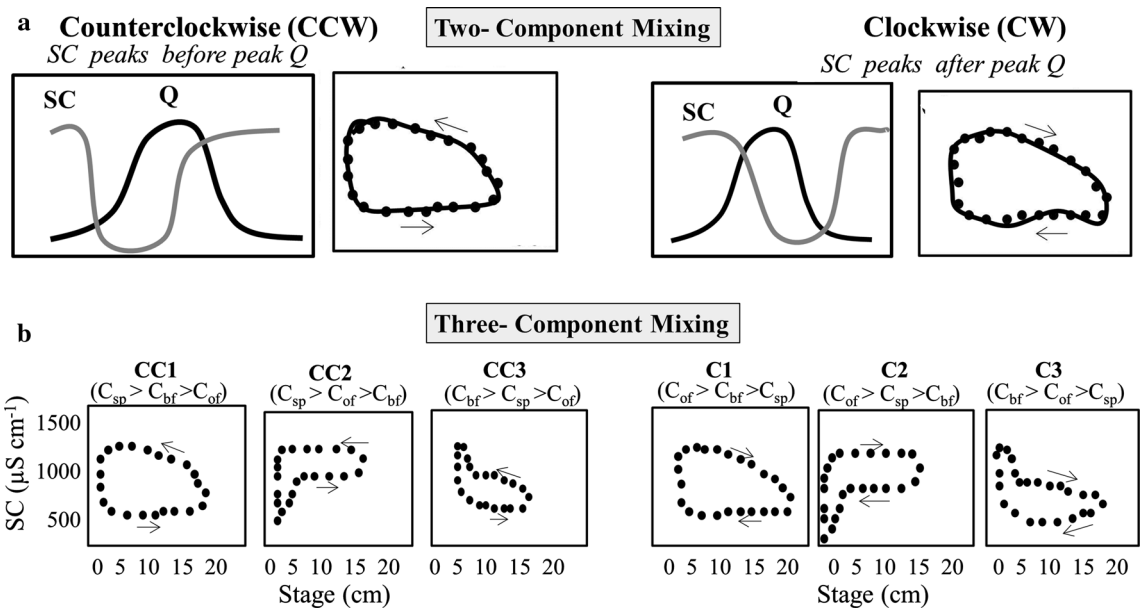

Fig. 1 Two-component (**a**) and three-component (**b**) mixing models based on SC–Stage hysteresis. Loop classifications include counterclockwise (*CCW*) and clockwise (*CW*) rotation, which can be subdivided into types CC1, CC2, CC3, C1, C2, and C3 (Evans and Davies 1998) based on relative SC concentrations of baseflow (*bf*), overland flow (*of*), and spoil water (*sp*)

is termed spoil water (*sp*) (Murphy et al. 2014). Overland flow describes water that did not infiltrate into the mine spoil materials and flowed into a stream as runoff, *bf* describes groundwaters (both local and regional) that may have come into contact with spoil materials or may source from areas that have not been mined, and *sp* describes water that has infiltrated and flowed through local mine spoils as matrix and preferential flows in the near-surface zone (Clark and Zipper 2016) or through voids and macropores deeper in the subsurface (Greer 2015; Guebert and Gardner 2001; Hawkins 2004). As Evans and Davies (1998) described, these three storm hydrograph components have different concentrations and discharge timing, and each component influences overall stream chemistry. Therefore, C–Q relationships can be categorized into differing hysteresis patterns that are interpreted to infer relative source contributions of chemical constituents.

Few studies have examined C–Q relationships in a surface mining context. Bonta (2004) used C–Q regressions to analyze three mining-influenced streams in Ohio, USA, and found significant relationships between streamwater chemical concentrations and discharge during the pre-disturbance and post-mining phases. Murphy et al. (2014) analyzed C–Q hysteresis in mining-influenced watersheds in Tennessee, USA, for 40 storms (1975–2009) and concluded that a continuous supply of dissolved ions from mining areas was the source of elevated TDS in the New River. Murphy et al. (2014), however, documented one watershed and two sub-basins within that watershed, and sampled >1 km downstream of mining activities where small fractions of upstream watersheds were disturbed by coal mining.

In order to improve understanding of TDS release from mining-influenced watersheds, more research is necessary. Using high temporal resolution (10–15 min. interval) sampling within 100 m of VF streamflow emergence, we analyzed SC, stage, and SC–Stage relationships for five VFs of varying ages in Virginia over 12 months. Specific objectives were to examine the differences in hydrochemical discharge patterns among VF streams and to compare relationships between SC and stage for VF streams on multiple time scales (i.e., storm event, seasonally). Results are intended to aid the understanding of stream discharge and TDS-generation pathways of mined landforms in watersheds with VFs.

Materials and methods

Site description

Five valley fills were selected for analysis; all sites were in two clusters in the Appalachian coalfields of southwestern Virginia (Fig. 2). Sites 1 and 4 were located in Dickenson County, VA, and sites 2, 3, and 5 were clustered in Wise County, VA (Table 1). Site numbering is by ascending age, ranging from ~2.5-years old (Site 1, which was partially constructed during the analysis period) to 20-years old (Site 5) at the time of data collection. All VFs were

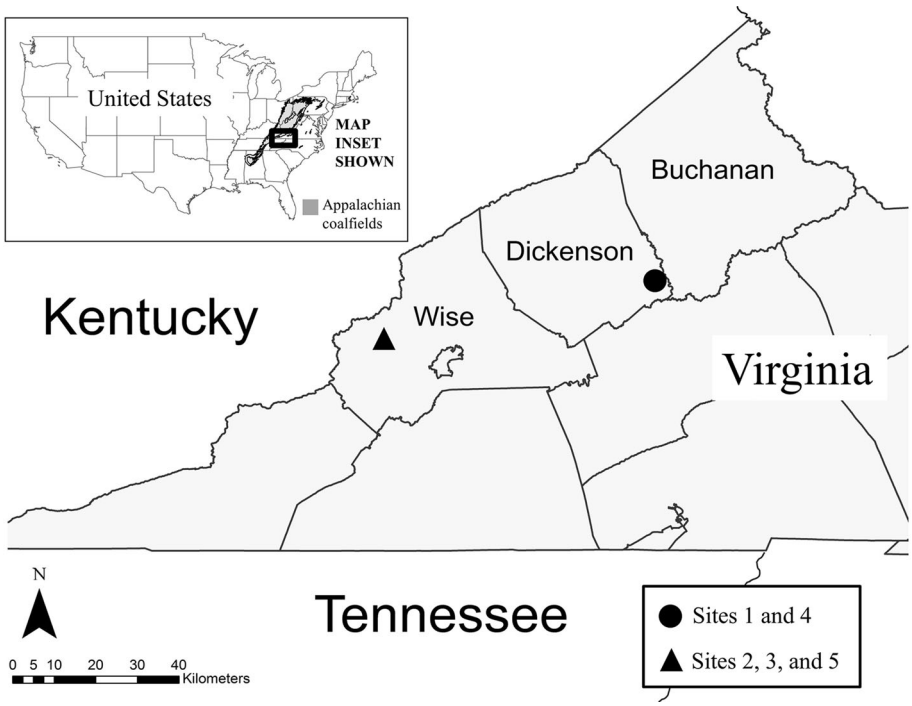

Fig. 2 Location map for Sites 1–5. The Appalachian coalfields are indicated by *gray coloration* on the US map

Table 1 Descriptions of basic site conditions

Site	Age (years)	County	VF surface area (m^2)	Vegetative cover	Storm event threshold (mm)
1[†]	2.5	Dickenson	13,540	Grassed	2.5
2	6	Wise	7540	Grassed	3.5
3	9	Wise	16,030	Immature forest, open canopy	4.0
4	15	Dickenson	11,650	Forested, closed canopy	1.5
5	20	Wise	7040	Immature forest, open canopy	2.5

[†] This valley fill had been under construction since mid-2012. At the time of data collection, the lower sections were complete and vegetated, but construction of upper sections was ongoing

constructed with Pennsylvanian-aged gray and brown sandstones of the Wise and Norton Formations (Meissner 1978; Nolde et al. 1986). Aerial imagery and geometric tools in ArcMap (v. 10.1, ESRI 2012: Redlands, CA) were used to estimate VF surface areas. Site 3 had the largest surface area, and Site 5 had the smallest surface area. The VFs at Sites 2–5 were constructed as V-shaped tiered structures using the loose-dump method which enables gravity-induced segregation of spoil materials such that larger rocks occur near the VF base where they form a rock drain that discharges water rapidly from the fill. At the time of data collection, Site 1 was being constructed of tiered lifts with the lower lifts of the VF completed and vegetated, but the upper lifts were still being constructed. Vegetative cover ranged from grass on the younger fills, to immature tree coverage without closed canopy on the medium-aged VFs, to closed canopy tree coverage on the oldest fills.

Data collection

Data collection was initiated on all sites on December 1, 2013, and extended on all but one site to November 30, 2014; Site 2 data collection was terminated on July 23, 2014, due to channel reconstruction by the cooperating mining firm. Daily precipitation data (mm) were obtained from the nearest National Climatic Data Center (NOAA 2016) weather stations (Grundy, VA for Sites 1 and 4; Norton, VA for Sites 2, 3, and 5). Automated data loggers recorded SC and stage data every 15 min at Sites 1 and 4, and every 10 min at Sites 2, 3, and 5. Data collection occurred within $\sim$100 m of streamflow emergence from the VF toes and above sedimentation ponds. Streams flowed continuously from all VF toes during the study period. Onset HOBO conductivity (HOBO U24-001, Bourne, MA, USA), and barometric pressure (HOBO U20-001-01) data loggers collected SC and stage data at Sites 1 and 4. Data at sites 2, 3, and 5 were collected with Solinst Levelogger Junior 3001 (Toronto, Canada) and Onset HOBO barometric pressure transducers.

Data processing included converting raw instrument output files to stage and SC in accordance to manufacturers' instructions. For Sites 1 and 4, SC data were corrected using HOBO software, and manual measurements taken with a handheld conductivity meter (Thermo Scientific Orion Star A122) during data collection. For other sites, SC was manually calibrated with standard solutions at three points (1413, 5000, and 12,880 $\mu s\ cm^{-1}$) then converted from the instrument reading via a linear regression line ($r^2 > 0.99$). Stage was determined using HOBO software, which converted pressure to stage using both air and submerged absolute pressures recorded by the automated data loggers.

Hydrologic analyses typically utilize stream discharge data; however, discharge data were not collected at most of these sites due to stream bed and bank instability, differences in watershed disturbance levels, and personnel travel time constraints. Prior studies have used stage, rather than discharge, in multiple types of hydrologic analyses (e.g., Herman et al. 2008; Magnusson et al. 2014; McMahon et al. 2003; Shuster et al. 2008), including hydrochemical storm event analysis (Miller and Drever 1977); thus, stage was used for all methods subsequently described.

Data analyses

Two analyses were conducted: (1) analysis of general VF stage and SC patterns (2) analysis of SC–Stage relationships via regression and hysteresis loop analyses. Summaries of these analyses were done seasonally (Winter: December–February, Spring: March–May, Summer: June–August, and Fall: September–November), and all data collected over the entire study period were also summarized.

General VF stage and SC patterns

In order to separate stormflow from baseflow periods, storm event discharge thresholds were determined for each site using a two stage process. First, cumulative distribution functions (CDFs) and histograms were created for all stage data collected at each site (Fig. 3). The CDFs were visually inspected for abrupt changes in slope, and those

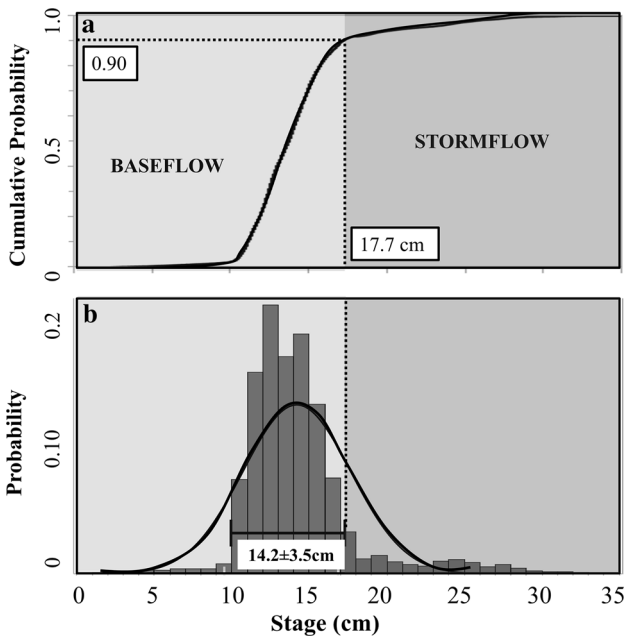

Fig. 3 Baseflow and stormflow separation technique using **a** cumulative density frequency analysis and **b** histogram mean + standard deviation for Site 2

change points were visually estimated. Second, storm event thresholds were then verified using histograms of the stage data, and data analyses revealed that the visually identified CDF thresholds were approximately equivalent to the mean + one standard deviation. Thus, storm event thresholds were defined for each VF as equivalent to one standard deviation of that VFs dataset (Table 1). Stormflow and baseflow SC and stage values were used to calculate seasonal means of SC and stage for each flow type.

SC–Stage regressions

Regression analyses were used to describe SC–Stage relationships. A power law regression, modified from Bonta (2004) to incorporate stage data, was defined as follows:

$$\mathrm{SC} = a\ (\mathrm{Stage})^{b} \quad (1)$$

where a is the coefficient parameter and b is the exponent parameter. Both SC and stage were log-transformed and a linear regression was performed. The resulting slope of the transformed linear regression is equivalent to the b exponent parameter, whereas the intercept is equivalent to the log of a.

SC–Stage hysteresis

Individual storm events were separated from the stage data record by first identifying exceedances of the storm event threshold for each VF (Table 1), separating storm sequences that exceeded the storm threshold, then adding observations recorded for 30 min prior to the initial exceedance. Such sequences were defined as a single storm event.

Bivariate plots of stage versus SC were created for all storm events (hereafter "storms"). Storms without hysteresis were classified as not applicable (NA), storms with a downward slope but no discernible loop direction were classified as downward sloping (DS), and storms with clearly evident hysteresis were classified as clockwise (CW) or counterclockwise (CCW) using a two-component model (Fig. 1a). For three-component hysteresis analysis based on the *bf, sp,* and *of* hydrograph components, CCW and CW loop types were classified as type 1, 2, or 3, and thus the possible storm classifications were as follows: CC1, CC2, CC3, C1, C2, or C3 (Evans and Davies 1998; Fig. 1b). Both two- and three-component storm hysteresis patterns were summarized for all data and seasonally. Hysteresis patterns were also summarized by vegetative period as either growing season (April 15–October 15) or non-growing season (October 16–April 14) based on regional climate data (Southeast Regional Climate Center 2016a, b).

Statistical analyses

Using JMP (v. 11.0, SAS Institute: Cary, N.C.), Kruskal–Wallis tests determined significant differences ($p \leq 0.05$) in baseflow and stormflow SC and stage seasonally, as well as significant differences in precipitation amounts associated with hysteresis loop classifications. Significant SC–Stage regressions were defined as those in which the slope was significantly different from zero ($p \leq 0.05$). Contingency tables and Chi-squared (χ^2) analyses identified statistical differences ($p \leq 0.05$) between the number of SC–Stage hysteresis loops by site, season, and vegetative period.

Results

General VF stage and SC patterns

Stage

Mean stage values ranged from 2.2 cm (Site 4) to 25.4 cm (Site 3), and maximum stages ranged from 18.6 cm (Site 4) to 55.3 cm (Site 3). Stages at all sites had clear seasonal influences (Table 2), and four of five sites had significantly higher stages in winter than any other season. Site 5 had the strongest seasonal effect; all four seasons had significantly different stages.

Table 2 Valley fill stream daily mean stage and specific conductance–stage regressions for Sites 1–5

Site (age)	Season	Stage (cm)	BF-Stage (cm)*	SF-Stage (cm)*	*a*	*b*	*p* (≤0.05)
1 (2.5 years)	Winter	7.0[a†]	6.3[a]	11.3[a]	1140	−1.50	<0.0001
	Spring	6.2[b]	6.1[b]	8.8[d]			NS[‡]
	Summer	5.2[c]	5.2[d]	10.0[b]			NS
	Fall	6.2[b]	5.9[c]	9.2[c]	1450	−1.69	<0.0001
	ALL	*6.2*	*5.9*	*9.7*	*1170*	*−1.48*	*<0.0001*
2 (6 years)	Winter	14.6[a]	14.0[a]	23.7[a]	1750	−1.51	0.0144
	Spring	15.0[a]	13.5[b]	22.0[b]	1090	−0.87	0.0048
	Summer	12.1[b]	12.0[c]	17.7[c]	1660	−1.63	<0.0001
	ALL	*14.2*	*13.3*	*22.7*	*1350*	*−1.19*	*0.0021*
3 (9 years)	Winter	31.0[a]	31.0[a]	34.9[a]	1320	−0.84	0.0349
	Spring	22.8[c]	22.8[d]	35.0[a]	1600	−1.24	0.0002
	Summer	23.6[b]	23.6[c]	28.2[c]	1900	−1.36	<0.0001
	Fall	24.2[b]	24.1[b]	29.2[b]	1910	−1.37	<0.0001
	ALL	*25.4*	*25.3*	*34.4*	*1770*	*−1.31*	*<0.0001*
4 (15 years)	Winter	2.9[a]	1.9[b]	6.3[a]	1630	−1.88	<0.0001
	Spring	2.3[b]	2.3[a]	2.8[d]	1950	−2.06	<0.0001
	Summer	1.5[c]	1.5[d]	4.4[c]	2060	−2.19	<0.0001
	Fall	1.9[bc]	1.7[c]	5.8[b]	2060	−2.23	<0.0001
	ALL	*2.2*	*2.0*	*4.1*	*1930*	*−2.10*	*<0.0001*
5 (20 years)	Winter	15.8[a]	14.7[a]	20.4[b]	1260	1.67	0.0003
	Spring	12.3[c]	12.1[c]	23.5[a]			NS
	Summer	11.3[d]	11.3[d]	15.3[d]	2750	−2.20	<0.0001
	Fall	14.6[b]	14.0[b]	18.1[c]	950	−1.23	0.0106
	ALL	*13.5*	*12.8*	*19.6*	*1680*	*−1.83*	*<0.0001*

* *BF* baseflow, *SF* stormflow, *SC* specific conductance

† Values followed by same letters within each site are not significantly different from one another ($p \leq 0.05$)

‡ *NS* SC-Stage regression not statistically significant ($p > 0.05$)

Mean baseflow stages were highest in winter (Table 2) and lowest in summer for four of the five sites. All sites had seasonal baseflow stage effects with all seasons having significantly different mean baseflow values. Mean stormflow stages ranged from 4.1 cm (Site 4) to 34.4 cm (Site 3), and seasonal effects were present at all five VFs. The largest stormflow stages occurred in winter for 4 of 5 sites.

Specific conductance

Minimum SCs measured were ~200 μS cm^{-1}, maximum SCs measured were >2000 μS cm^{-1}, and mean baseflow SCs ranged from 790 μS cm^{-1} (Site 5) to 1660 μS cm^{-1} (Site 4) (Fig. 4). Seasonal effects on baseflow SC were present at all sites. Summer had the largest mean baseflow SC, and winter had the smallest mean baseflow SC at 3 of 5 sites. Site 5 had the largest season-to-season range of baseflow SCs (350 μS cm^{-1}) which occurred between summer and winter, whereas Site 3 had the smallest season-to-season range of baseflow SCs (160 μS cm^{-1}).

Mean stormflow SCs ranged from 490 μS cm^{-1} (Site 5) to 1450 μS cm^{-1} (Site 4) and were generally lower than baseflow SCs (Fig. 4). Seasonal effects on stormflow SC occurred at all sites; spring had significantly larger stormflow SCs at 3 of 5 sites. Site 4 had the largest season-to season range in stormflow SCs, with a range of >450 μS cm^{-1} between spring (1640 μS cm^{-1}) and winter (1160 μS cm^{-1}), whereas Site 1 had the smallest season-to-season range (140 μS cm^{-1}).

SC–Stage relationships

SC–Stage regressions

All sites had significant regressions for the full study period (Fig. 5). Site 4 had the most negative *b* constant (−2.10), and Site 2 had the least negative (−1.19), with more negative *b* constants (Eq. 1) indicating a greater dilution of SC during stormflow. The regression *a* parameter value (intercept, Eq. 1) was largest at Site 4 (1930 μS cm^{1}) and

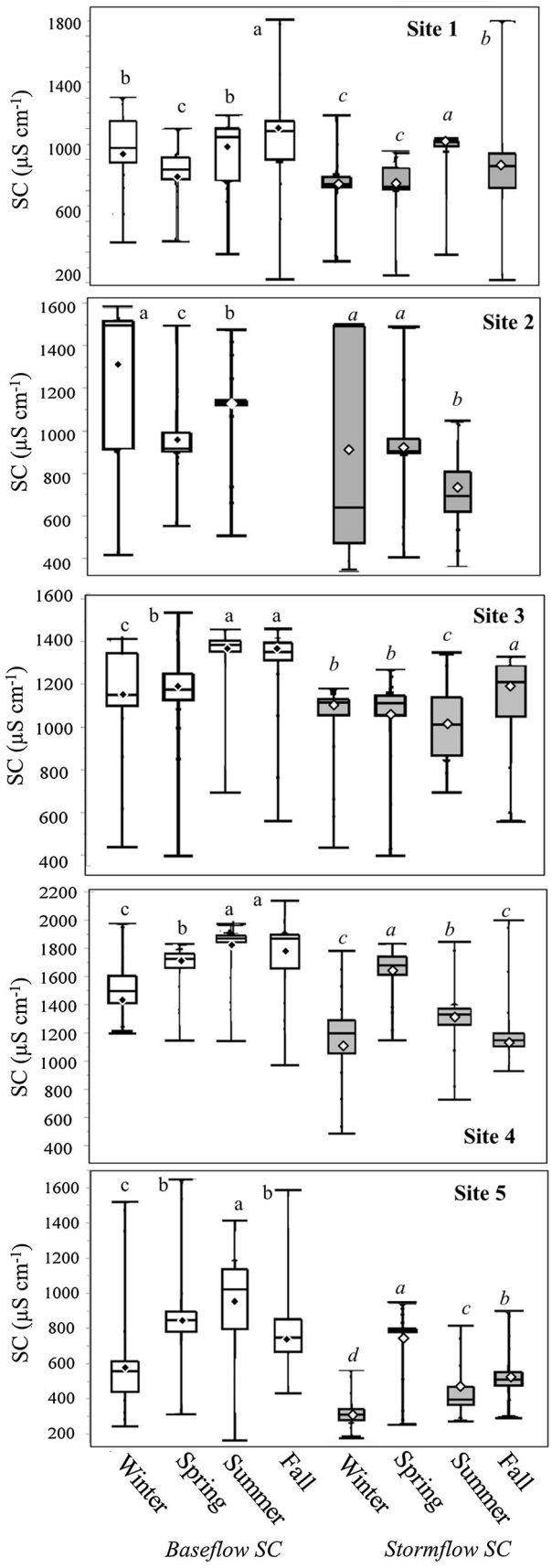

◀**Fig. 4** *Boxplots* illustrating the range of baseflow (*white*) and stormflow (*gray*) SCs in Sites 1–5. *Wide* bars represent the minimum, 25th percentile, median, 75th percentile, and maximum values, respectively. *Diamonds* represent means. Baseflow and stormflow SC is classified by season. For each flow type, *boxplots* with *different letters* indicate significant differences between seasons ($p \leq 0.05$). Note differences in *y*-axis scales

smallest at Site 1 (1170 µS cm^1), with larger *a* values implying greater potential SC during baseflow.

Sixteen of the 19 seasonal SC–Stage regressions were statistically significant (Table 2). Seasonal *b* parameter values ranged from −2.23 to −0.87, and seasonal *a* parameter values ranged from 950 to 2750 µS cm^1. Seasonal regressions varied in significance by site. Site 1 had only two significant seasons, and Site 5 had three significant seasons. Sites 2, 3, and 4 had significant SC–Stage regressions for all seasons. All five VFs had significant SC–Stage regressions for fall and winter, whereas spring flows had the fewest significant regressions (3 of 5).

SC–Stage hysteresis

A total of 97 storms were identified and analyzed across all VFs. Storm totals for individual VFs ranged from 14 (Site 4) to 30 storms (Site 5) (Table 3). Winter had the largest number (31 in December, January, and February), and summer had the smallest number (17 in June, July, August) of storms. Excluding Site 4, which only had storms of a single hysteresis type, more storms occurred during the growing season (43 storms) than in the non-growing season (40 storms). Larger precipitation events occurred in summer and winter (25 and 21 mm, respectively) than in fall (18 mm on average) and spring (12 mm on average), and seasonal rainfall averages were largest in summer and fall (12 mm on average for the entire season) and smaller in winter (10 mm) and spring (7 mm).

Precipitation events had clear signatures in the hydrographs, and the patterns of SC during storms were generally the inverse of stage (Fig. 6), with SC at high concentrations during baseflow, diluting to a minimum during stormflow, and gradually increasing in SC as the system returned to baseflow conditions.

Of the 97 storms analyzed, 67 (70 %) showed hysteresis effects, and 30 (30 %) did not (Table 3). Approximately one-third of the storms had CW hysteresis patterns, one-third had CCW hysteresis patterns, and the last third had no hysteresis effects (Fig. 6). Of the 30 storms without hysteresis effects, 18 had DS patterns, and 12 were classified as NA, thus only 12 % of the total 97 storms analyzed had a random SC–Stage relationship. Storms without hysteresis occurred in response to smaller precipitation events (13 mm, on average) than CW and CCW storms.

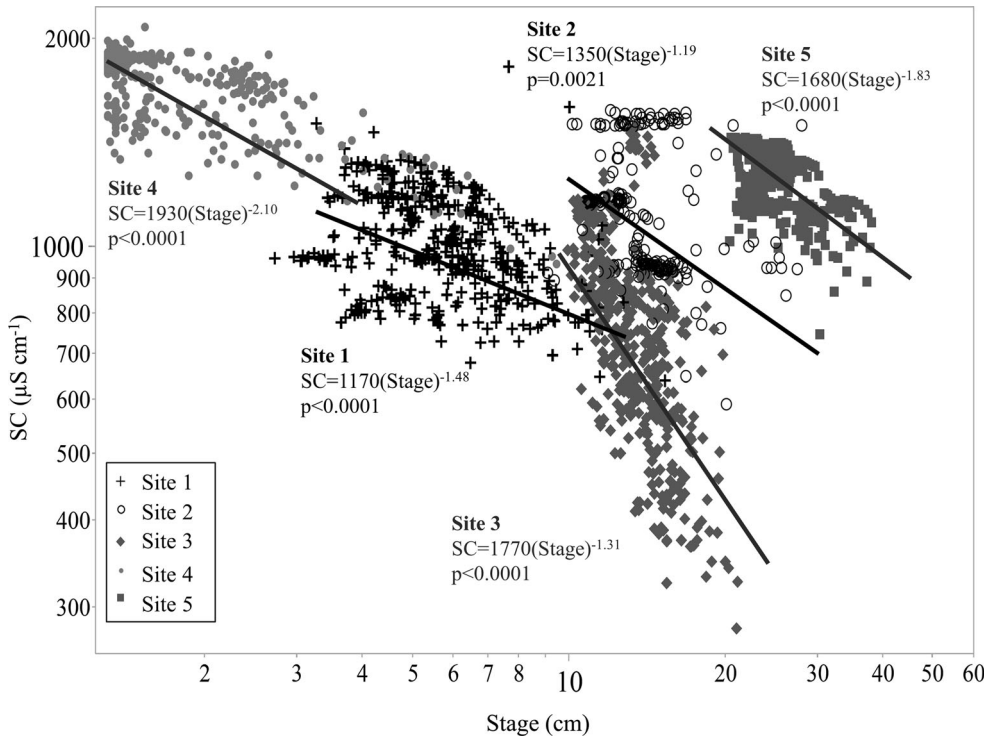

Fig. 5 Full year regressions showing significant relationships between SC and stage in Sites 1–5

Table 3 Summary of specific conductance–stage hysteresis loop patterns (Fig. 1) by site, season and vegetative period

	Clockwise (n = C1, n = C3)	Counterclockwise (n = CC1, n = CC3)	No hysteresis (n = DS*, n = NA*)	Total
Site (age)	Numbers of storms			
1 (2.5 years)	11 (3, 8)	6 (0, 6)	1 (0, 1)	18
2 (6 years)	2 (1, 1)	6 (0, 6)	8 (4, 4)	16
3 (9 years)		11 (3, 8)	8 (3, 5)	19
4 (15 years)	14 (6, 8)			14
5 (20 years)	6 (0, 6)	11(4, 7)	13 (11, 2)	30
Total	*33 (10, 23)*	*34 (7, 27)*	*30 (18, 12)*	*97*
Season	Numbers of storms			
Winter	6 (1, 5)	21 (4, 17)	4 (1, 3)	31
Spring	10 (5, 5)	7 (3, 4)	12 (4, 8)	29
Summer	5 (0, 5)	3 (0, 3)	9 (9, 0)	17
Fall	12 (4, 8)	3 (0, 3)	5 (4, 1)	20
Vegetation period	Numbers of storms			
Growing season[†‡]	17^{a}	7^{b}	19^{a}	43
Non-growing season[†‡]	2^{b}	27^{a}	11^{b}	40
Mean precipitation (mm)[§]	17^{b}	22^{a}	13^{b}	

* *DS* downward sloping, *NA* no trend/random

† Storm event counts followed by different letters are significantly different ($p \leq 0.05$)

‡ Growing and non-growing season storm counts exclude Site 4 storms

§ Precipitation values followed by different letters are significantly different ($p \leq 0.05$)

For two-component model analysis, CCW rotation occurred for 34 storms, whereas CW rotation occurred for 33 of the 67 storms with hysteresis. Precipitation for CCW storms (22 mm, on average) was significantly greater ($p \leq 0.05$) than for CW storms (17 mm, on average). Site 4 only had CW storms, and Site 3 did not have any CW

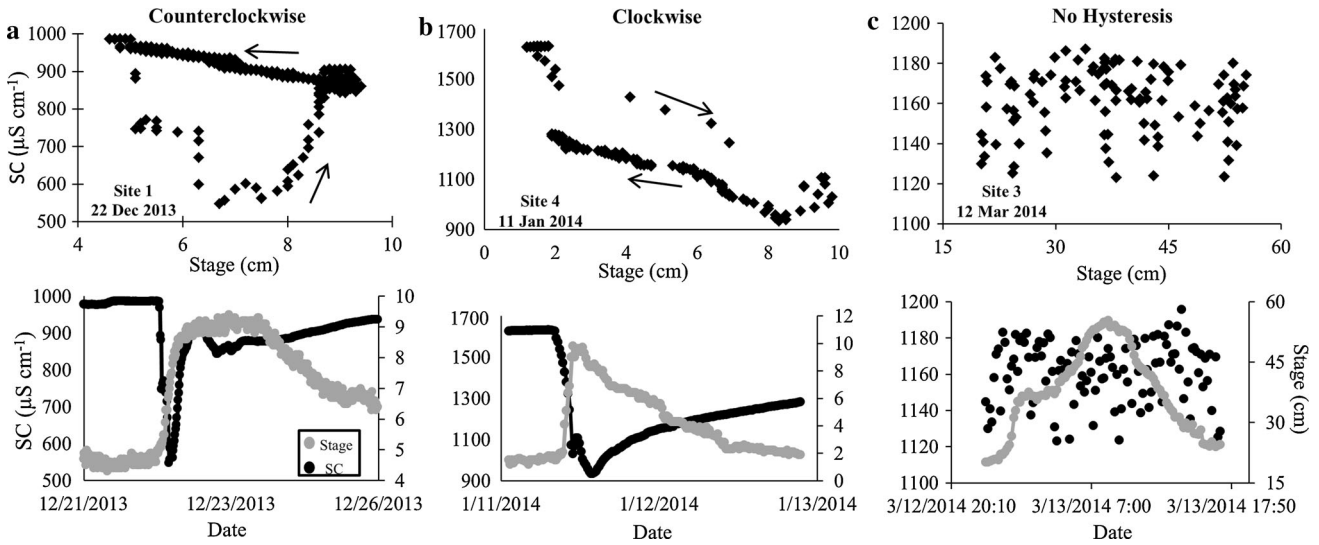

Fig. 6 Examples of SC–Stage bivariate plots and associated hydrographs for individual precipitation events with **a** counterclockwise rotation, **b** clockwise rotation and **c** no hysteresis

storms. All other sites had both CW and CCW storms. Site 1, the youngest, had the fewest storms without hysteresis, whereas Site 5, the oldest, had the most storms without hysteresis. Winter had more storms with CCW than with CW or no hysteresis. Significantly, more CW storms occurred during the growing season ($p \leq 0.05$), whereas significantly more CCW storms occurred during the non-growing season ($p \leq 0.05$).

For three-component model analysis, no C2 or CC2 hysteresis patterns were identified for any storm analyzed (Fig. 1). Types C1 and C3 patterns occurred in 10 and 23 storms, respectively, whereas CC1 and CC3 patterns occurred in 7 and 27 storms, respectively (Table 3). The most common hysteresis pattern of all storms was CC3, which occurred in 27 storms and was associated with significantly higher precipitation amounts (24 mm) than any other classification ($p \leq 0.05$). Type C3, CC3, and DS storms occurred in all seasons, C1 and NA occurred in all seasons except summer, and CC1 only occurred in winter and spring. Winter was the season most-dominated by a single-loop type, as 21 of the 31 winter storms had CC3 patterns.

Discussion

Analyses of VF stream stage, SC, and SC–Stage relationships revealed a pattern of relatively high SC during baseflow periods and dilution as a mechanism that reduced relative SC levels during stormflow periods. This general pattern was exhibited by all methods of analysis; mean stormflow SCs were lower than baseflow SCs in all sites and seasons, negative SC–Stage regressions implied dilution of SCs at higher stage conditions, and most storm hysteresis loops displayed a decrease in SC relative to a rise in stage.

Baseflow SCs ranged from $\sim$500 µS cm^{-1} to >2200 µS cm^{-1}, which is consistent with other studies on VF streams (Evans et al. 2014; Hartman et al. 2005; Pond et al. 2008, 2014). All seasonal baseflow and stormflow SC averages were >500 µS cm^{-1} except for winter and summer stormflow in Site 5 (360 and 450 µS cm^{-1}, respectively), indicating that SCs were generally above the 500 µS cm^{-1} level described by Pond et al. (2008) as a threshold above which detrimental aquatic macroinvertebrate community effects occur, and well above the 300 µS cm^{-1} level described by Cormier et al. (2013) as a threshold above which 5 % of aquatic genera are extirpated.

A prior study of 137 VFs in Virginia indicated that 19.6 ± 6.6 years after the initiation of VF construction may be required for SC in VF streams to decline to <500 µS cm^{-1} (Evans et al. 2014). However, the number of years since initial disturbance was not a predictor of mean discharge SC (Evans et al. 2014), and no association between VF age and discharge SC was found in a study of four VFs in West Virginia (Merricks et al. 2007). In our study, no age effect on SC was apparent as Site 5, the oldest VF (20 years), had the lowest mean SC (790 µS cm^{-1}) and Site 4 (15 years) had the highest mean SC (1660 µS cm^{-1}). Collectively, these results indicate that VF-stream SCs are variable with age, thus other factors must also influence SC. A factor known to influence SC levels in discharge is mine spoil properties (i.e., rock type, weathering extent, mineralogy), as mine spoils have varying potentials to produce SC (Daniels et al. 2016; Orndorff

et al. 2015); hence, the types of mine spoils used to construct VFs may have a greater influence on SCs than VF age. Internal VF structure and flow path configuration may also influence SCs, as VFs may differ in their capacity to store and transmit waters; however, such observations have been suggested but not documented by other studies (Miller and Zegre 2014; Evans et al. 2015; Greer 2015).

SC–Stage regressions

Significant SC–Stage regression parameters in all sites indicated that VFs and their contributing watersheds, which were predominantly mining influenced for all VFs studied, serve as sources of TDS to mining-influenced streams. Sites with more negative *b* parameters coupled with larger *a* values indicated higher SCs in baseflow that became more dilute during stormflow relative to other VFs. Such patterns are likely influenced by different geologic materials and spoil compositions used in VF construction, differences in VF construction methods, as well as differing channel configurations in the VF streams, hence the separation of individual VFs as shown in Fig. 5. Seasonal SC–Stage relationships also differed among VFs, implying that in addition to spoil composition differences, streamwater SCs were influenced to an extent by seasonally dependent factors, likely including vegetative cover and evapotranspiration (ET).

Prior studies on three streams in Ohio (Bonta 2004) and two streams in Tennessee (Murphy et al. 2014) also found significant SC–Q relationships in mining-influenced streams. Regression *a* parameters in this study (950–2750 μS cm^{-1}) were larger than the Bonta (2004) parameter values (168–629 μS cm^{-1}) and Murphy et al. (2014) parameter values (89–378 μS cm^{-1}). Differences in parameter values are likely due to differing geologies and TDS production potentials, but could also be due to sampling locations being ≥1000 m downstream of streamflow emergence for both studies (Bonta 2004; Murphy et al. 2014). Differences could also be due to sampling locations occurring below sedimentation ponds (Bonta 2004), which increases the likelihood of SC dilution from other source waters or tributaries. Although Bonta (2004) and Murphy et al. (2014) analyzed discharge rather than stage, most SC–Q regressions had negative slopes like those documented in this study, suggesting that mining-influenced watersheds across the Appalachian region serve as sources of TDS to streamwater and that SC is diluted at relatively high stages.

Storm event hysteresis

Hysteresis occurred in a majority of storm events analyzed, with all sites exhibiting multiple storm classifications (CC1, CC3, C1, C3). Hysteresis patterns varied with precipitation amounts and season, as CCW storms tended to occur in association with higher precipitation amounts and during winter, whereas CW storms tended to occur in association with lower precipitation amounts and during the growing season.

Considering VF streams, we assumed that overland flow (*of*) waters generally had lower SCs than baseflow (*bf*) and spoil waters (*sp*) due to limited contact time with spoil materials, and due to the highly leached nature of surface spoils that have been subjected to repeated contact with precipitation waters. We also assumed that *bf* waters for most VFs had relatively constant SCs during a given storm event, although this assumption may not hold for Sites 1 and 4 where *bf* is known to include underground mine water discharges. On all VFs, it was assumed that *sp* water flows occur in response to precipitation infiltration into the VF, which generates TDS via spoil–water interactions within the VF interior. These assumptions described above were used to interpret observed hysteresis patterns.

Counterclockwise hysteresis patterns (Fig. 6a) are characterized by a greater influence of dilute waters during the hydrograph's rising limb and an increased influence of higher SC waters during the falling limb, suggesting that dilute *of* waters have a strong influence on SC during the initial storm response. The fact that CCW hysteresis occurred during significantly larger storm events (22 mm on average) supports this explanation, suggesting that CCW hysteresis occurred in response to rapid runoff of dilute *of* waters during the precipitation event. Large precipitation events are more likely to exceed VF-surface infiltration capacities than storms with smaller amounts of rainfall (Jorgensen and Gardner 1987), causing event water, which has limited contact with VF spoils to dominate the hydrograph's rising limb. After such dilution, the stormflow shifts to apparent dominance by higher SC waters, specifically *sp* and/or *bf* waters, during the hydrograph's falling limb. Also, CCW hysteresis occurred more often in winter relative to other seasons, implying a climatic influence. Colder winter temperatures and minimal vegetative cover cause reduced ET and enable increased soil moisture relative to summer months, perhaps reducing infiltration and increasing *of* waters. Frozen soil surfaces may also have contributed to increase *of* for some storms.

Clockwise hysteresis patterns (Fig. 6b) are characterized by delayed SC dilution relative to the rise in stage during a storm, and their interpretation is not as direct. Significantly, more CW storms occurred during the growing season, thus one possible interpretation is that CW storms may flush easily soluble surface salts that were brought to the surface via ET processes. Prior studies have found high cation concentrations in the top 5 cm of a mine soil (Nash et al. 2016), salt accumulation within spoil materials placed in

field leaching lysimeters (Daniels et al. 2016; Ross 2015), as well as visible salt accumulation on the surface of coal refuse piles (Daniels et al. 2010). Surficial salt accumulation may also occur on VF mine spoils and is likely influenced by seasonal wetting and drying cycles and ET during drier periods. Accumulated surficial salts may be flushed as high SC *of* waters during the initial stages of precipitation events, resulting in relatively high SC in the initial *of* runoff during a storm. Subsequent *of* waters would be more dilute relative to the initial flush of surface salts, enabling the CW hysteresis pattern to occur.

More complex explanations for CW storms are also possible. Site 4 generated CW hysteresis for all storms, suggesting that the hydrology of this site is unique. As described above, *bf* waters in Site 4 include underground mine discharges, which appear to be responsive to surface hydrologic events. Although underground, the mining conduits are located above the VF and relatively close to the surface, and may discharge high-TDS waters that have been stored in the underground mine complex for a period of time, resulting in relatively high SCs during the hydrograph's rising limb of CW hysteresis.

Another possible explanation for CW rotation involves the rapid flushing of *sp* waters. A prior study demonstrated that mine spoil fill surfaces can be highly heterogeneous and can contain zones that are porous and promote rapid infiltration (Clark and Zipper 2016). Similarly, Greer (2015) found rapid rainwater infiltration into a VF, which was followed by rapid downward movement of the wetting front along preferential flowpaths within the VF. These studies suggest the presence of subsurface properties resembling "pseudokarst" features, i.e., highly permeable materials with inter-connected subsurface channels, and voids that enable rapid throughflow (Caruccio and Geidel 1995; Hawkins and Aljoe 1990). Miller and Zegre (2014) suggested that such pseudokarst features may occur within loose-dumped VFs such as those in this study. Pseudokarst features may enable infiltrated water to become *sp* water that travels rapidly through the VF, either mobilizing readily soluble salts or displacing stored or pre-event water (McDonnell 1990) with relatively high SCs. If such *sp* waters were to dominate the initial phase of a given storm response, the result would be relatively high SC waters discharged during the hydrograph's rising limb and CW hysteresis.

Overall, hysteresis patterns in the five VF streams were influenced by storm event size, seasonal climate variation, and growing season. A prior study on mining-influenced streams in Tennessee, USA, similarly concluded that storm event size influenced hysteresis patterns, as Murphy et al. (2014) found that CCW (CC2) patterns occurred when peak flow was $<25\ m^3\ s^{-1}$ and CW (C3) patterns occurred when peak flow was $>25\ m^3\ s^{-1}$. In contrast, our results suggested that storms with higher precipitation amounts tended to have CCW rotation, whereas smaller storms tended to have CW hysteresis. Furthermore, no CC2 patterns were identified for any of the 97 storms in this analysis. Discrepancies between our results and Murphy et al. (2014), as well as the Bonta (2004) C–Q regression analyses indicate that mining-influenced streams vary chemically and hydrologically between sites, but also by sampling location within the watershed (i.e., upstream vs. downstream) and seasonally. Results, therefore, highlight the importance of sampling directly at the emergence of VF streamflow to fully characterize the "mining signature" in discharges and water chemistry of VF streams.

Conclusion

The hydrochemistry of five streams emerging from Appalachian VFs varied by season, precipitation amounts during storm events, and among VFs. Stream stage and SC patterns, SC–Stage regressions, and storm hysteresis indicated high SCs during baseflow with dilution of SC during stormflow. Seasonal climatic factors such as antecedent moisture conditions, frozen soil surfaces, and evapotranspiration rates also appear to influence VF hydrologic responses and stream hydrochemistry. Future research should include chemical analysis of source waters (spoil water, overland flow, and groundwater) in order to understand the specific chemistry of each source water component, as well as the interaction of all three source waters during baseflow and stormflow. Storm hysteresis analysis of specific ions may also help to more fully understand VF hydrochemistry and the sources of TDS in VF streams.

Acknowledgments The authors would like to thank the cooperating mining firms, Dan Evans, and Dr. Trip Krenz for site access and data collection. This research was sponsored by the Appalachian Regional Initiative for the Environmental Sciences (ARIES), Virginia Tech Institute for Critical Technology and Applied Sciences, Powell River Project, Virginia Agricultural Experimental Station, Wells Fargo through the Clean Technology and Innovation Grant Program, and the USDA Hatch Program of the National Institute of Food and Agriculture. The opinions expressed herein are solely those of the authors and do not imply endorsement by ARIES or Wells Fargo employees.

References

Atanackovic N, Dragisic V, Stojkovic J, Papic P, Zivanovic V (2013) Hydrochemical characteristics of mine waters from abandoned mining sites in Serbia and their impact on surface water quality. Environ Sci Pollut Res 20:7615–7626

Boehme EA, Zipper CE, Schoenholtz SH, Soucek DJ, Timpano AJ (2016) Temporal dynamics of benthic macroinvertebrate communities and their response to elevated specific conductance in Appalachian coalfield headwater streams. Ecol Indic 64:171–180

Bonta JV (2004) Concentration–discharge regression parameters in watersheds of varying lithology subjected to surface coal mining and reclamation. J Soil Water Conserv 59:86–101

Caruccio FT, Geidel G (1995) Status report: long-term effects of alkaline trenches and funnels at the mercer site. West Virginia Surface Mine Drainage Task Force Symposium, Morgantown

Clark EV, Zipper CE (2016) Vegetation influences near-surface hydrological characteristics on a surface coal mine in eastern USA. Catena 139:241–249

Cormier SM, Suter GW, Zheng L (2013) Derivation of a benchmark for freshwater ionic strength. Environ Toxicol Chem 32:263–271

Daniels WL, Stewart B, Zipper CE (2010) Reclamation of coal refuse disposal areas. Virginia Cooperative Extension Publication 460-131

Daniels WL, Zipper CE, Orndorff CW, Skousen JG, Barton CD, McDonald L, Beck M (2016) Predicting total dissolved solids release from central Appalachian coal mine spoils. Environ Pollut 216:371–379

ESRI (Environmental Systems Resource Institute) (2012) ArcMap 10.1. ESRI, Redlands, CA

Evans C, Davies C (1998) Causes of concentration/discharge hysteresis and its potential as a tool for analysis of episode hydrochemistry. Water Resour Res 34:129–137

Evans DM, Zipper CE, Donovan P, Daniels WL (2014) Long-term trends of specific conductance in waters discharged by coal-mine valley fills in central Appalachia, USA. J Am Water Resour Assoc 50:1449–1460

Evans DM, Zipper CE, Hester ET, Schoenholtz S (2015) Hydrologic effects of surface coal mining in Appalachia (USA). J Am Wat Resour Assoc 51(5):1436–1452

Greer BM (2015) Electrical resistivity imaging of preferential flow through surface mine valley fills with comparisons to other land forms. Thesis, Virginia Polytechnic Institute and State University

Guebert MD, Gardner TW (2001) Macropore flow on reclaimed surface mines: infiltration and hillslope hydrology. Geomorphology 39:151–169

Hartman KJ, Kaller MD, Howell JW, Sweka JA (2005) How much do valley fills influence headwater streams? Hydrobiologia 532:91–102

Hawkins JW (2004) Predictability of surface mine spoil hydrologic properties in the Appalachian plateau. Ground Water 42:119–125

Hawkins JW, Aljoe JA (1990) Hydrologic characterization and modeling of a heterogeneous acid-producing surface coal mine spoil, Upshur County, WV. Proceedings of the National Symposium of Mining, University of Kentucky, pp 43–52

Herman EK, Toran L, White WB (2008) Threshold events in spring discharge: evidence from sediment and continuous water level measurement. J Hydrol 351:98–106

House WA, Warwick MS (1998) Hysteresis of the solute concentration/discharge relationship in rivers during storms. Water Resour 32:2279–2290

Huang X, Sillanpaa M, Gjessing E, Peraniemi S, Vogt R (2010) Environmental impacts of mining activities on the surface water quality in Tibet: Gyana valley. Sci Total Environ 408:4177–4184

Jorgensen DW, Gardner TW (1987) Infiltration capacity of disturbed soils: temporal change and lithologic control. Water Resour Bull 23:1161–1172

Lewis WM, Grant MC (1979) Relations between stream discharge and yield of dissolved substances from a Colorado mountain watershed. Soil Sci Soc Am J 128:353–363

Lindberg TT, Bernhardt ES, Bier R, Helton AM, Merola RB, Vengosh A, DiGiulio RT (2011) Cumulative impacts of mountaintop mining on an Appalachian watershed. Proc Nat Acad Sci USA 108:20929–20934

Magnusson J, Kobierska F, Huxol S, Hayashi M, Jonas T, Kirchner JW (2014) Melt water driven stream and groundwater stage fluctuations on a glacier forefield. Hydrol Process 28:823–836

McDonnell J (1990) A rationale for old water discharge through macropores in a steep, humid catchment. Water Resour Res 26:2821–2832

McMahon G, Bales JD, Coles JF, Giddings EM, Zappia H (2003) Use of stage data to characterize hydrologic conditions in an urbanizing environment. J Am Water Resour Assoc 39:1529–1546

Meissner CR (1978) Geologic map of the Duty quadrangle, Dickenson, Russell, and Buchanan Counties, Virginia. US Geological Survey, Geologic Quadrangle Map GQ-1458

Merricks TC, Cherry DS, Zipper CE, Currie R, Valenti T (2007) Coal-mine hollow fill and settling pond influences on headwater streams in southern West Virginia, USA. Environ Monit Assess 129:359–378

Messinger T, Paybins KS (2003) Relations between precipitation and daily and monthly mean flows in gaged, unmined and valley-filled watersheds, Ballard Fork, West Virginia, 1999–2001 USGS Report WRi no. 2003-4113

Miller WR, Drever JI (1977) Water chemistry of a stream following a storm, Absaroka Mountains, Wyoming. Geol Soc Am Bull 88:286–290

Miller AJ, Zegre NP (2014) Mountaintop Removal Mining and Catchment Hydrology. Water 6:472–479

Murdoch PS, Shanley JB (2006) Detection of water quality trends at high, median, and low flow in a Catskill Mountain stream, New York, through a new statistical method. Water Resour Res 42:W08407

Murphy JC, Hornberger JM, Liddle RG (2014) Concentration–discharge relationships in the coal mined region of the New River basin and Indian Fork sub-basin, Tennessee, USA. Hydrol Process 28:718–728

Nash WL, Daniels WL, Haering KC, Burger JA, Zipper CE (2016) Long-term effects of rock type on Appalachian coal mine spoil properties. J Environ Qual. doi:10.2134/jeq2015.10.0540

National Oceanic and Atmospheric Administration (NOAA) (2016) National centers for environmental information. Climate Data Online. http://www.ncdc.noaa.gov/cdo-web/

Negley T, Eshleman K (2006) Comparison of stormflow responses of surface-mined and forested watersheds in the Appalachian mountains, USA. Hydrol Process 20:3467–3483

Nolde JE, Lovett JA, Whitlock WW, Miller RL (1986) Geology of the Norton quadrangle, Virginia. Virginia Division of Mineral Resources, Publication 65

Orndorff ZW, Daniels WL, Zipper CE, Eick M, Beck M (2015) A column evaluation of Appalachian coal mine spoils' temporal leaching behavior. Environ Pollut 204:39–47

Phillips JD (2004) Impacts of surface mine valley fills on headwater floods in eastern Kentucky. Environ Geol 45:367–380

Pond GJ, Passmore ME, Borsuk FA, Reynolds L, Rose CJ (2008) Downstream effects of mountaintop coal mining: comparing biological conditions using family- and genus-level macroinvertebrate bioassessment tools. J N Am Benthol Soc 27:717–737

Pond GJ, Passmore ME, Pointon ND, Felbinger JK, Walker CA, Krock KJ, Fulton JB, Nash WL (2014) Long-term impacts on macroinvertebrates downstream of reclaimed mountaintop mining valley fills in central Appalachia. Environ Manag 54:919–933

Rice KC, Chanat JG, Hornberger GM, Webb JR (2004) Interpretation of concentration–discharge patterns in acid-neutralizing capacity during storm flow in three small, forested catchments in Shenandoah National Park, Virginia. Water Resour Res 40:W05301

Ross LC (2015) Effect of leaching scale on prediction of total dissolved solids release from coal mine spoils and refuse. M.S. Thesis, Virginia Polytechnic Institute and State University

Shuster WD, Zhang Y, Roy AH, Daniel FB, Troyer M (2008) Characterizing storm hydrograph rise and fall dynamics with stream stage data. J Am Water Resour Assoc 44:1431–1440

Skousen JG, Sexstone A, Ziemkiewicz PF (2000) Acid mine drainage control and treatment. In: Barnhisel RI et al (eds) Reclamation of drastically disturbed lands. Agronomy monographs. #41. ASA, CSSA, and SSSA, Madison, WI, pp 131–168

Southeast Regional Climate Center (2016a) Spring freeze possibilities (Jan. –Jul. 31): Wise, VA. http://www.sercc.com/cgi-bin/sercc/cliMAIN.pl?va9215

Southeast Regional Climate Center (2016b) Fall freeze possibilities (Jul. 31-Dec. 31): Wise, VA. http://www.sercc.com/cgi-bin/sercc/cliMAIN.pl?va9215

Stump DE (2001) Customized techniques for interpretation of suspended sediment data. In: Proceedings of the seventh federal interagency sedimentation conference, Reno NV, pp 12–19

Timpano AJ, Schoenholtz SH, Zipper CE, Soucek DJ (2010) Isolating effects of total dissolved solids on aquatic life in central appalachian coalfield streams. In: Proceedings, national meeting of the American society of mining and reclamation, Pittsburgh, PA, pp 1284–1302

Timpano AJ, Schoenholtz SH, Soucek DJ, Zipper CE (2015) Salinity as a limiting factor for biological condition in mining-influenced Central Appalachian headwater streams. J Am Water Resour Assoc 51:240–250

US EPA (2003) Mountaintop mining/valley fills in Appalachia draft programmatic environmental impact statement. EPA 9-03-R-00013

US EPA (2011) The effects of mountaintop mines and valley fills on aquatic ecosystems of the central Appalachian coalfields. EPA/600/R-09/138F

Walling DE, Webb BW (1980) The spatial dimension in the interpretation of stream solute behavior. J Hydrol 47:129–149

Williams GP (1989) Sediment concentration versus water discharge during single hydrologic events in rivers. J Hydrol 111:89–106

Younger PL, Wolkersdorfer C (2004) Mining impacts on the fresh water environment: technical and managerial guidelines for catchment scale management. Mine Water Environ 23:2–80

Zipper CE, Burger JA, McGrath JM, Rodrigue JA, Holtzman GI (2011) Forest restoration potentials of coal-mined lands in the eastern United States. J Environ Qual 40:1567–1577